Letter | Editors' Suggestion

Importance of nonlinear long-range electron-phonon interaction for the carrier mobility of anharmonic halide perovskites

Matthew Houtput,[1] Ingvar Zappacosta,[1] William Wenborn,[1] Serghei Klimin,[1] Samuel Poncé,[2,3] Jacques Tempere,[1] and Cesare Franchini[4,5]

[1]*Theory of Quantum Systems and Complex Systems, Universiteit Antwerpen, B-2000 Antwerpen, Belgium*
[2]*European Theoretical Spectroscopy Facility and Institute of Condensed Matter and Nanosciences, Université Catholique de Louvain, Chemin des Étoiles 8, B-1348 Louvain-la-Neuve, Belgium*
[3]*WEL Research Institute, avenue Pasteur 6, 1300 Wavre, Belgium*
[4]*Faculty of Physics, Computational Materials Physics, University of Vienna, Kolingasse 14-16, A-1090 Vienna, Austria*
[5]*Department of Physics and Astronomy, Alma Mater Studiorum - Università di Bologna, 40127 Bologna, Italy*

(Received 12 March 2026; revised 10 September 2026; accepted 16 September 2026; published 8 October 2026)

The interaction between the electrons and the lattice vibrations in a solid is responsible for various important effects, such as formation of polarons, temperature-dependent band gaps, phonon-limited carrier transport, and conventional superconductivity. Most works assume a linear electron-phonon interaction, where the electron only interacts with one phonon at a time. However, the validity of this assumption has not been verified in polar anharmonic materials, where large ionic displacements may invalidate the assumption of linear interaction. Here, we show that nonlinear electron-phonon interactions contribute significantly to the finite-temperature electron mobility of the inorganic lead halide perovskite $CsPbI_3$. The effect of nonlinear interaction is taken into account using the recently derived expression for the long-range part of the one-electron-two-phonon matrix element. We calculate the electron mobility from first principles within the self-energy relaxation-time approximation, treating the electron-phonon coupling in the long-range approximation. Despite these approximations, the calculated mobilities are in good agreement with the available experimental data, while enabling us to isolate and quantify the contribution of nonlinear electron-phonon interactions relative to the conventional linear coupling. We find that the one-electron-two-phonon interaction modifies the temperature dependence of the mobility in $CsPbI_3$ and reduces its room-temperature value by about 10%. This sizable contribution results from the combined effects of strong lattice anharmonicity and large thermal phonon populations, the latter being enhanced by the low phonon frequencies associated with the heavy constituent atoms. These results identify a regime in which nonlinear electron-phonon interactions become relevant and indicate that they should be explicitly considered for finite-temperature properties of anharmonic halide perovskites.

DOI: 10.1103/jl6h-yzky

Halide perovskites [1] are known for their excellent optoelectronic properties [2–4]. This has led to their usage in the development of several promising technological applications, such as solar cells [5–7] and energy-efficient lighting [8,9]. A particularly important property in the context of these applications is the charge transport [10], usually quantified by the carrier mobility μ. A deeper understanding of the microscopic processes that govern mobility is therefore desirable.

In most materials, this microscopic understanding can be found from the theory of phonon-limited transport [11]. One assumes that the charge carriers can interact with harmonic phonons with frequencies $\omega_{\mathbf{q}\nu}$, through a linear electron-phonon scattering process as shown in Fig. 1(a). Then, a common way to calculate the carrier mobility μ is to calculate the electron energies $\varepsilon_{\mathbf{k}n}$, phonon frequencies $\omega_{\mathbf{q}\nu}$, and electron-phonon matrix elements $g_{mn\nu}(\mathbf{k},\mathbf{q})$ from first principles [12], and use these to solve the linearized Boltzmann transport equation for the carrier mobility [11]. However, many of the assumptions in this theory are not applicable to most halide perovskites. For example, it has been shown that several of the halide perovskites are strongly anharmonic [13–17], requiring a treatment with renormalized phonon frequencies and spectral broadening, or even the full phonon spectral function. It has also been suggested that the quasiparticle picture might not be valid in halide perovskites [15], requiring a treatment beyond the Boltzmann transport equation [18]. The violation of these common assumptions makes comparison with experimental measurements of the mobility [19–27] difficult.

We show here that another common assumption is violated in halide perovskites: the assumption of linear electron-phonon interaction. This approximation is often made out of necessity, as the electron-phonon matrix elements for higher-order electron-phonon interactions such as the one in Fig. 1(b) are not known. Regardless, it has been predicted that some halide perovskites get significant contributions to the band gap renormalization from nonlinear electron-phonon interaction [28,29].

In this Letter, we quantify the effect of the nonlinear one-electron-two-phonon interaction on the carrier mobility of cesium lead iodide ($CsPbI_3$), a representative inorganic halide perovskite. There have been several treatments of

 ©2026 American Physical Society

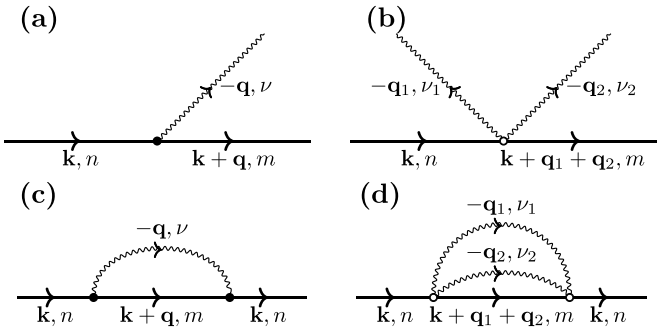


FIG. 1. (a) and (b) Feynman diagrams for the linear and lowest-order nonlinear electron-phonon interaction. In (a), the long-range approximation amounts to $\mathbf{q} \to \mathbf{0}$, and in (b) it amounts to $-\mathbf{q}_1 \to \mathbf{q}_2$. (c) and (d) Contributions to the imaginary part of the retarded self-energy that are taken into account in this article, where (c) is the Fan-Migdal diagram, and (d) is its nonlinear analog. We do not include the Debye-Waller diagram since it is real.

nonlinear electron-phonon interaction in the literature in recent years [30–39], but most focus on lattice model Hamiltonians [40–56]. We note that nonlinear interaction should not be confused with higher-order treatments of the linear interaction, such as those which include the crossing diagrams [57,58]. In order to treat the nonlinear interaction from first principles, we use the recently derived expression for the dipole long-range part of the one-electron-two-phonon matrix element $g_{mn\nu_1\nu_2}(\mathbf{k}, \mathbf{q}_1, \mathbf{q}_2)$ [59]. All material properties that enter this matrix element can be calculated from first principles. Since the linear electron-phonon interaction in $CsPbI_3$ is dominated by the long-range contribution [10,25,60], we expect this analysis to be representative for the full nonlinear one-electron-two-phonon interaction in $CsPbI_3$. We investigate the accuracy of the long-range approximation further in Sec. S3 of the Supplemental Material [61] (see also Refs. [62,63] therein).

Our aim is to establish physical criteria for determining when nonlinear electron-phonon interactions can be safely neglected and when they must be taken into account. Such criteria provide a useful framework for assessing previous and future calculations of halide perovskites that include only linear electron-phonon coupling [10,16,17,64]. To this end, we investigate the relative contributions of the linear and nonlinear electron-phonon interaction to the carrier mobility in the cubic phase of $CsPbI_3$. In order to use the theory derived in Ref. [59], we use the harmonic and quasiparticle approximations. As discussed, these are likely poor approximations in $CsPbI_3$. Furthermore, we calculate the mobility using the self-energy relaxation time approximation (SERTA), rather than solving the linearized Boltzmann Transport Equation (BTE) iteratively. While these approximations may affect the absolute values of the calculated mobilities, they provide a consistent framework for assessing the relative importance of linear and nonlinear electron-phonon scattering. Reassuringly, the resulting mobilities are also in good agreement with the available experimental data. Potential directions for a relaxation of these assumptions are discussed at the end of the manuscript.

The drift electron mobility μ_e can be computed with the linearized BTE [11]:

$$\mu_{e,\alpha\beta} = \frac{-e}{n_e(2\pi)^3} \sum_{n\in\mathrm{CB}} \int_{1\mathrm{BZ}} \mathrm{d}^3\mathbf{k}\, v_{\mathbf{k}n\alpha}\, \partial_{E_\beta} f(\varepsilon_{\mathbf{k}n}). \tag{1}$$

Here $\alpha, \beta \in \{x, y, z\}$ represent Cartesian directions, e is the elementary charge, n_e is the electron density, $\hbar\mathbf{k}$ is the crystal momentum and is restricted to the first Brillouin zone (1BZ), n labels the electron bands restricted to the conduction bands, $\varepsilon_{\mathbf{k}n}$ are the electron band energies, and $v_{\mathbf{k}n\alpha} = \frac{1}{\hbar}\frac{\partial\varepsilon_{\mathbf{k}n}}{\partial k_\alpha}$ are the band velocities. Finally, the most important quantity that appears in Eq. (1) is the out-of-equilibrium occupation function $\partial_{E_\beta} f(\varepsilon_{\mathbf{k}n})$ due to an applied electric field E_β applied in the direction β.

In the SERTA [65], the out-of-equilibrium electronic occupation functions reduce to

$$\partial_{E_\beta} f(\varepsilon_{\mathbf{k}n}) = \frac{\partial f^0(\varepsilon_{\mathbf{k}n})}{\partial\varepsilon_{\mathbf{k}n}} v_{\mathbf{k}n\beta}\tau_{\mathbf{k}n}, \tag{2}$$

Here, $f^0(\varepsilon)$ is the equilibrium occupation function for the electrons, which is the Fermi-Dirac distribution. Additionally, $\tau^{-1}_{\mathbf{k}n}$ are the scattering rates of the electrons with the phonons [11], which can be obtained from the on-shell retarded diagonal electron self-energy $\Sigma^{\mathrm{R}}_{\mathbf{k}nn}$ [11]:

$$\frac{1}{\tau_{\mathbf{k}n}} = -\frac{2}{\hbar}\mathrm{Im}\big[\Sigma^{\mathrm{R}}_{\mathbf{k}nn}(\varepsilon_{\mathbf{k}n})\big]. \tag{3}$$

If we were to only use the linear electron-phonon interaction, we would be able to use the standard expression for the Fan-Migdal self-energy from Fig. 1(c), written in terms of $\varepsilon_{\mathbf{k}n}$, $\omega_{\mathbf{q}\nu}$, and $g_{mn\nu}(\mathbf{k}, \mathbf{q})$ [11]. In that case, the BTE has also been derived [11] and implemented [66], but this is not the case for the Hamiltonian that contains a nonlinear electron-phonon matrix element $g_{mn\nu_1\nu_2}(\mathbf{k}, \mathbf{q}_1, \mathbf{q}_2)$. The advantage of using SERTA is that it only requires the self-energy, so we avoid having to rederive and reimplement the BTE. Instead, we can use the long-range theory from Ref. [59], where the retarded self-energy was calculated up to lowest order in the electron-phonon interaction. This gives the Fan-Migdal self-energy, Fig. 1(c), and a similar term due to the nonlinear electron-phonon interaction in Fig. 1(d) [59]:

$$\begin{aligned}\Sigma^{\mathrm{R}}_{\mathbf{k}nn}(\varepsilon_{\mathbf{k}n}) = \frac{\hbar e^2}{\varepsilon_0(2\pi)^3}\int_0^{+\infty}\mathrm{d}\omega\int_{\mathbb{R}^3}\mathrm{d}^3\mathbf{Q}\frac{\mathbf{Q}\cdot\boldsymbol{\mathcal{P}}(\omega)\cdot\mathbf{Q}}{(\mathbf{Q}\cdot\boldsymbol{\varepsilon}^\infty\cdot\mathbf{Q})^2}\\ \times\left[\frac{1-f^0(\varepsilon_{\mathbf{k}+\mathbf{Q}n})+n(\hbar\omega)}{\varepsilon_{\mathbf{k}n}-\varepsilon_{\mathbf{k}+\mathbf{Q}n}-\hbar\omega+i\delta}\right.\\ \left.+\frac{f^0(\varepsilon_{\mathbf{k}+\mathbf{Q}n})+n(\hbar\omega)}{\varepsilon_{\mathbf{k}n}-\varepsilon_{\mathbf{k}+\mathbf{Q}n}+\hbar\omega+i\delta}\right].\end{aligned} \tag{4}$$

In this expression, $n(\hbar\omega)$ is the Bose-Einstein distribution for phonons, and $\mathbf{Q} = \mathbf{q} + \mathbf{G}$ represents a phonon momentum extended to the entire reciprocal space $\mathbb{R}^3$: This is equivalent to an integral over $\mathbf{q} \in 1\mathrm{BZ}$ and a sum over reciprocal lattice vectors $\mathbf{G}$. We note that the integral over $\mathbf{Q}$ should decay quickly and approximately vanish at the boundary of the first Brillouin zone in order for the long-range approximation to be valid, so in practice it is irrelevant whether the integration domain is $\mathbb{R}^3$ or 1BZ. $\boldsymbol{\varepsilon}^\infty$ and $\boldsymbol{\mathcal{P}}(\omega)$ are material-specific 3×3 tensors: ε^∞_{ij} is the high-frequency dielectric tensor, and

$\mathcal{P}_{ij}(\omega)$ is a dimensionless spectral function which represents the strength of the long-range electron-phonon interaction. For both tensors, the Cartesian directions i and j refer to the direction of a constant electric field $\mathcal{E}_i$ or $\mathcal{E}_j$ which is induced by the conduction electrons. Using the theory from Ref. [59], the electron-phonon spectral function can be calculated as a sum of two contributions. The first contribution is $\mathcal{T}_{ij}(\omega)$, which is the contribution from the one-electron-two-phonon interaction. It originates from the diagram in Fig. 1(d), and is a continuous spectral function which is defined as [59]

$$\mathcal{T}_{ij}(\omega) \equiv \frac{e^2}{2\hbar\varepsilon_0(2\pi)^3}\sum_{\nu_1\nu_2}\int_{1\mathrm{BZ}} \mathrm{d}^3\mathbf{q} Y_{\nu_1\nu_2 i}(\mathbf{q}) Y^*_{\nu_1\nu_2 j}(\mathbf{q}) \times \{[1+n(\hbar\omega_{\mathbf{q}\nu_1})+n(\hbar\omega_{\mathbf{q}\nu_2})]\delta(\omega-|\omega_{\mathbf{q}\nu_1}+\omega_{\mathbf{q}\nu_2}|) + |n(\hbar\omega_{\mathbf{q}\nu_2})-n(\hbar\omega_{\mathbf{q}\nu_1})|\delta(\omega-|\omega_{\mathbf{q}\nu_1}-\omega_{\mathbf{q}\nu_2}|)\}. \tag{5}$$

In this expression, $Y_{\nu_1\nu_2 i}(\mathbf{q})$ represents the strength of the long-range interaction between an electron and two phonons, in branches ν_1, ν_2 and with approximately opposite momenta $-\mathbf{q}_1 \approx \mathbf{q}_2 = \mathbf{q}$. It is given in terms of the phonon frequencies $\omega_{\mathbf{q}\nu}$ and eigenvectors $e_{\kappa\alpha\nu}(\mathbf{q})$, and the derivative of the dynamical matrix with respect to the induced electric field $\frac{\partial \mathcal{D}_{\kappa\alpha,\kappa'\beta}(\mathbf{q})}{\partial \boldsymbol{\mathcal{E}}}$ [59]:

$$Y_{\nu_1\nu_2 i}(\mathbf{q}) \equiv \frac{1}{ie}\sqrt{\frac{\hbar}{2\omega_{\mathbf{q}\nu_1}}\frac{\hbar}{2\omega_{\mathbf{q}\nu_2}}} \times \sum_{\kappa\alpha\kappa'\beta} e^*_{\kappa\alpha\nu_1}(\mathbf{q})\frac{\partial \mathcal{D}_{\kappa\alpha\kappa'\beta}(\mathbf{q})}{\partial \mathcal{E}_i} e_{\kappa'\beta\nu_2}(\mathbf{q}). \tag{6}$$

In this manuscript, we focus on the cubic phase of $CsPbI_3$. In this case, $\boldsymbol{\varepsilon}^\infty$, $\boldsymbol{\mathcal{P}}(\omega)$, and $\boldsymbol{\mathcal{T}}(\omega)$ all reduce to scalars [59]:

$$\varepsilon^\infty_{ij} = \varepsilon^\infty \delta_{ij}, \tag{7}$$

$$\mathcal{P}_{ij}(\omega) = \mathcal{P}(\omega)\delta_{ij}, \tag{8}$$

$$\mathcal{T}_{ij}(\omega) = \mathcal{T}(\omega)\delta_{ij}. \tag{9}$$

Since these tensors only have a single independent component, it is sufficient to align the electric field $\boldsymbol{\mathcal{E}}$ along only one of the three Cartesian axes. In this manuscript, we arbitrarily choose $\boldsymbol{\mathcal{E}}$ along the z direction, meaning that we calculate $\mathcal{T}(\omega) \equiv \mathcal{T}_{zz}(\omega)$ by setting $i = j = z$ in Eq. (5).

The second contribution is $\mathcal{R}(\omega)$, which is the Fröhlich-type contribution from the linear electron-phonon interaction [67–69]. It is a sum of delta functions at the longitudinal optical phonon frequencies ω_ν at $\mathbf{q} = \mathbf{0}$ [59]:

$$\mathcal{R}(\omega) \equiv \frac{e^2}{2\varepsilon_0\Omega_0}\sum_\nu \frac{|p_\nu|^2}{\omega_\nu}\delta(\omega-\omega_\nu), \tag{10}$$

where Ω_0 is the size of the unit cell and p_ν is the mode polarity, which represents the strength of the long-range interaction between an electron and one phonon branch ν with momentum $\mathbf{q} \approx \mathbf{0}$ [59]. Once both contributions are known, $\mathcal{P}(\omega)$ is simply evaluated as the sum of the two:

$$\mathcal{P}(\omega) = \mathcal{R}(\omega) + \mathcal{T}(\omega). \tag{11}$$

We note that $\mathbf{q}$ is not restricted to $\mathbf{q} \approx \mathbf{0}$ in Eqs. (5) and (6). Therefore, to calculate the nonlinear spectral function $\mathcal{T}(\omega)$ using Eq. (5), we need the phonon frequencies over the entire first BZ [see also Fig. 2(b)], despite making the long-range approximation [59]. This is counterintuitive because for the familiar linear electron-phonon interaction, only phonons with $\mathbf{q} \approx \mathbf{0}$ contribute to Eq. (10).

The p_ν in Eq. (10) can be written in terms of the Born effective charge tensor and phonon eigenvectors [59,61], and $Y_{\nu_1\nu_2 z}(\mathbf{q})$ can be written in terms of phonon frequencies and eigenvectors as well as their derivative with respect to an external electric field [59]. All of these can be calculated from first principles (see Sec. S2 in the Supplemental Material [61] and Refs. [70–75] therein), which allows to evaluate the self-energy in Eq. (4). Finally, in order to compute the electron mobility in Eq. (1), we need an expression for the electron bands $\varepsilon_{\mathbf{k}n}$. At sufficiently low carrier densities, only the electronic states close to the conduction band minimum will contribute. Around the conduction band minimum, $CsPbI_3$ has a single parabolic conduction band:

$$\varepsilon_{\mathbf{k}} = \frac{\hbar^2|\mathbf{k}|^2}{2m^*_e}, \tag{12}$$

where we take $m^*_e = 0.17 m_{\mathrm{el}}$ for the effective band mass of the electron [10]. We note that at low carrier densities, the hole mobility is calculated with a similar equation as Eq. (1) for the electrons, except that we need to use the effective hole mass $m^*_h = 0.16 m_{\mathrm{el}}$ [10]. Ultimately, the effective band mass m^* only enters the mobility as a prefactor according to $\mu \sim (m^*)^{-\frac{3}{2}}$ (see also Eq. (S31) in the Supplemental Material [61]). Therefore, we only need to calculate the electron mobility: The carrier mobility $\mu \equiv \mu_e + \mu_h$ can then be obtained as $\mu = \mu_e[1 + (m^*_e/m^*_h)^{3/2}]$.

Figure 2 shows the material properties of cubic $CsPbI_3$ needed for the retarded self-energy in Eq. (4), calculated from first principles using the method described in Ref. [59]. These material properties include the phonon frequencies $\omega_{\mathbf{q}\nu}$, the one-electron-two-phonon strengths $Y_{\nu_1\nu_2 z}(\mathbf{q})$, and the electron-phonon spectral function $\mathcal{P}(\omega) = \mathcal{R}(\omega) + \mathcal{T}(\omega)$. Additionally, we have calculated $\varepsilon^\infty = 5.96$ for the dielectric tensor of $CsPbI_3$, close to other first principles calculations in the literature [10,76]. The phonon calculations, with and without external electric field, were all performed in the harmonic approximation at zero temperature. This means that there are imaginary phonon modes in Fig. 2, since the cubic phase is only stabilized by anharmonic effects at finite temperatures [77]. At lower temperatures, the tetragonal or orthorhombic phases are stable. However, due to the computational cost of a larger unit cell with an external electric field, we are limited to the cubic phase. To calculate the nonlinear electron-phonon spectral function $\mathcal{T}(\omega)$ in Fig. 2(c), we set $Y_{\nu_1\nu_2 z}(\mathbf{q}) = 0$ for all branches with frequencies $\omega_{\mathbf{q}\nu} < 0.1$ THz in order to circumvent the imaginary branches. The value

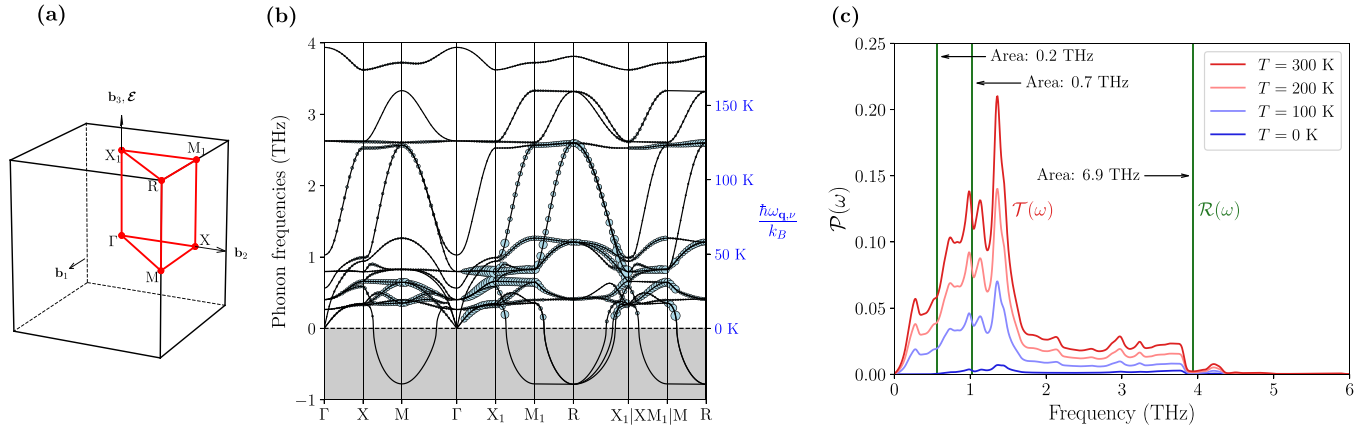


FIG. 2. First principles results for the nonlinear electron-phonon properties of $CsPbI_3$ in the cubic phase. (a) High-symmetry Brillouin zone path for a simple cubic material, with an electric field breaking the symmetry in the z direction. (b) Phonon frequencies $\omega_{\mathbf{q}\nu}$ of cubic $CsPbI_3$ at zero temperature. The overlaid circles have areas proportional to $\sum_{\nu'} |Y_{\nu\nu' z}(\mathbf{q})|^2$, i.e., the magnitude of the long-range interaction strengths $|Y_{\nu\nu' z}(\mathbf{q})|^2$ between the phonon $(\mathbf{q}\nu)$ and all other phonons of the form $(-\mathbf{q}\nu')$. There are imaginary phonon modes because the cubic phase is unstable at zero temperature: We set $Y_{\nu\nu',z}(\mathbf{q}) = 0$ for any branches with $\omega_{\mathbf{q},\nu} < 0.1$ THz. (c) One-electron-two-phonon spectral function $\mathcal{T}(\omega)$ calculated from Eq. (5) and the data from (b). $\mathcal{R}(\omega)$ is shown as a sequence of vertical lines representing the Dirac delta functions, with the areas under the delta functions indicated for reference. The effect of the one-electron-two-phonon interaction is significantly enhanced at finite temperatures: This is ultimately due to the very low phonon frequencies of $CsPbI_3$ (see main text).

0.1 THz is arbitrarily chosen; later, we show results with the cutoff varying from 0.05 to 0.2 THz to show that the qualitative conclusions are independent of this choice. It is not straightforward to determine how the imaginary modes would modify the nonlinear electron-phonon spectral function $\mathcal{T}(\omega)$ if they were treated within an anharmonic phonon theory. Two competing effects are expected. On the one hand, including additional phonon branches would increase $\mathcal{T}(\omega)$, since each branch contributes positively to Eq. (5). On the other hand, anharmonic renormalization generally shifts phonon frequencies upward, thereby reducing the Bose-Einstein occupation factors $n(\hbar\omega_{\mathbf{q}\nu})$ entering Eq. (5). The net effect on $\mathcal{T}(\omega)$ is therefore not known *a priori*. Nevertheless, we expect the present calculation to capture the correct order of magnitude of the nonlinear electron-phonon contribution.

Importantly, the linear electron-phonon spectral function $\mathcal{R}(\omega)$ is independent of temperature, whereas the nonlinear electron-phonon spectral function $\mathcal{T}(\omega)$ depends on temperature through the Bose-Einstein distributions $n(\hbar\omega_{\mathbf{q}\nu})$. At sufficiently large temperatures $k_B T \gg \hbar\omega_{\mathbf{q}\nu}$, the Bose-Einstein distribution satisfies $n(\hbar\omega_{\mathbf{q}\nu}) \approx \frac{k_B T}{\hbar\omega_{\mathbf{q}\nu}} - \frac{1}{2}$ so that Eq. (5) scales linearly with temperature. $CsPbI_3$ has low phonon frequencies, so all phonons are thermally activated at room temperature. Additionally, Fig. 2(b) shows that most of the contributions to $\mathcal{T}(\omega)$ come from phonons with frequencies lower than 1 THz. Therefore, we see a strong temperature dependence in Fig. 2(c). Although $\mathcal{T}(\omega)$ is very small at zero temperature, it is of order 0.1 at room temperature, which means one needs to look at finite temperature properties of $CsPbI_3$ in order to see the effect of nonlinear interaction. A similar result is seen for the temperature-dependent band gap renormalization in methylammonium lead iodide ($MAPbI_3$) [28].

With the electron-phonon spectral function $\mathcal{P}(\omega)$ from Fig. 2, we can calculate the SERTA carrier mobility from Eqs. (1)–(12) (see also Sec. S1 in the Supplemental Material [61] and Refs. [78,79] therein). Figure 3 shows the calculated carrier mobility. In line with the results of Fig. 2, the effects of nonlinear electron-phonon interaction are only revealed at higher temperatures. Above room temperature, the electron mobility in $CsPbI_3$ is reduced by about 10% by the long-range one-electron-two-phonon interaction. Additionally, the temperature dependence of $\mathcal{T}(\omega)$ in Fig. 2(c) changes the temperature scaling of the mobility. In the region between 140 and 500 K, the mobility is described by a power-law fit $\mu \sim T^{-\gamma}$, but the nonlinear electron-phonon interaction increases the exponent from $\gamma = 0.89$ to $\gamma = 0.97$.

In a previous work [59], we have shown that the contribution of the nonlinear interaction to the polaron ground-state energy is only 0.013% in the harmonic semiconductor LiF, and only 0.077% in the anharmonic perovskite $KTaO_3$. The much larger, ∼10% contribution found here for the mobility of $CsPbI_3$ arises from the combined action of three factors. First, the strong anharmonicity of $CsPbI_3$ leads to large ionic displacements and therefore the nonlinear coupling matrix elements $Y_{\nu\nu' i}(\mathbf{q})$ in Eq. (5) are larger than in LiF or $KTaO_3$. Second, mobility is a finite-temperature property, so thermal phonon populations amplify the nonlinear contribution through the Bose-Einstein factors $n(\hbar\omega_{\mathbf{q}\nu})$ in Eq. (5). Third, the low phonon frequencies associated with the heavy constituent atoms of $CsPbI_3$ result in large phonon occupations at room temperature over a broad range of modes. The nonlinear contribution is therefore expected to become appreciable when strong anharmonicity, finite-temperature phonon populations, and low-energy phonons occur simultaneously. Conversely, if one or more of these conditions is absent, as in LiF or $KTaO_3$, nonlinear electron-phonon effects are expected to remain small. This provides a simple physical criterion for identifying materials and finite-temperature properties for which nonlinear electron-phonon interactions may need to

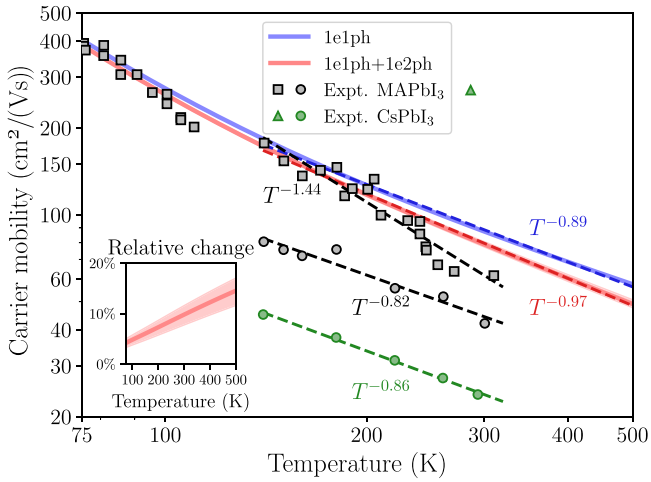


FIG. 3. SERTA carrier mobility of $CsPbI_3$ as a function of temperature, calculated using Eqs. (S16) and (S31) of the Supplemental Material [61] and the data from Fig. 2. The solid blue line is calculated using only the linear electron-phonon interaction from Eq. (10), and the solid red line is calculated including the one-electron-two-phonon interaction from Eq. (5). The inset shows the relative change of the mobility due to the one-electron-two-phonon interaction, relative to the mobility when nonlinear interaction is neglected. Calculations are performed using a frequency cutoff of 0.1 THz; the red shaded area shows the result when this cutoff is varied between 0.05 and 0.2 THz, indicating that the nonlinear contribution remains significant regardless of this cutoff value. Symbols indicate experimental mobility measurements in $CsPbI_3$ (green) and $MAPbI_3$ (gray): Squares denote single crystal THz conductivity measurements [25], circles denote thin film time-resolved microwave conductivity measurements [22], and the triangle denotes a thin film optical pump measurement [26]. Dashed lines indicate power-law fits in the region between 140 and 500 K.

be explicitly included, in particular in anharmonic halide perovskites.

To assess both the strengths and limitations of our long-range model, we compare our results with a first-principles calculation including both long- and short-range linear electron-phonon interactions (Fig. S4 of the Supplemental Material [61]) and with experimental mobility measurements for $CsPbI_3$ and methylammonium lead iodide ($MAPbI_3$) [22,25,26]. The mobility of $MAPbI_3$ provides a useful reference because it is likewise largely governed by Pb and I displacements [10,22,80]. As shown in Fig. 3, the measured mobilities exhibit considerable scatter; we therefore first compare their temperature dependence through the power-law relation $\mu \sim T^{-\gamma}$. The linear long-range model yields $\gamma = 0.89$, in good agreement with thin-film measurements ($\gamma = 0.82$; $\gamma = 0.86$). However, transport in polycrystalline thin films can be strongly affected by grain boundaries, which are not included in our model. A more direct comparison is therefore provided by single-crystal measurements. In this case, the absolute mobility values are comparable to our calculations, whereas the experimental temperature exponent, $\gamma = 1.44$, is larger than predicted by the linear long-range model. Notably, including the nonlinear electron-phonon interaction shifts the calculated temperature dependence toward the experimental value. In Sec. S3 of the Supplemental Material [61], we further compare the linear long-range model with a full first-principles calculation using the complete linear matrix elements $g_{mnv}(\mathbf{k}, \mathbf{q})$, evaluated on $144 \times 144 \times 144$ $\mathbf{k}$-grid and $\mathbf{q}$-grid. The full calculation gives $\gamma = 1.16$, confirming that the long-range approximation does not fully reproduce the temperature scaling, while yielding similar absolute mobility values. Thus, the approximations adopted here provide a reasonable estimate of the mobility magnitude and, more importantly, do not alter our central conclusion that nonlinear electron-phonon interactions reduce the mobility by approximately 10%. The remaining discrepancy with the experiment is likely due to the difference between the cubic and orthorhombic phases, the neglect of anharmonicity and one-electron-n-phonon nonlinear interaction terms with $n \geqslant 3$, the long-range approximation, or the use of the SERTA.

The present work suggests many perspectives for further research, several of which consist of improving the approximations made in this Letter. These perspectives can be separated into two distinct categories: improving the calculation of $\mathcal{P}(\omega)$, and using a more refined theory for electronic transport. Firstly, the calculation of $\mathcal{P}(\omega)$ can be improved by including phonon anharmonicity and all orders of one-electron-n-phonon interactions. Most notably, the results in Figs. 2 and 3 are based on the harmonic approximation for the phonons, but $CsPbI_3$ is known to exhibit strong phonon anharmonicity [77]. Since higher-order nonlinear interactions will involve higher powers of the Bose-Einstein occupation factors, they are expected to scale even faster with temperature than the linear and one-electron-two-phonon interaction. Depending on the prefactors associated with each of these terms, this scaling may significantly affect the power-law scaling of electron mobility at room temperatures, similarly to the result that Fig. 3 shows for the one-electron-two-phonon interaction.

The second category of perspectives is to take any result for the long-range electron-phonon spectral function $\mathcal{P}(\omega)$ as given, and use it to calculate the electron mobility with more advanced transport theories. One may start from the self-energy in Eq. (4), written in terms of $\mathcal{P}(\omega)$ and the harmonic quantities $\varepsilon_{\mathbf{k}n}$ and ε^{∞}. This expression can be used instead of the Fan-Migdal self-energy to derive the equivalent Boltzmann transport equation [11], or even more general transport theories that do not make the quasiparticle approximation [18,81]. This may significantly affect the results for the mobility, even given the same spectral function $\mathcal{P}(\omega)$.

We have shown that carrier mobility in $CsPbI_3$ receives a sizable contribution from nonlinear one-electron-two-phonon interactions, which are commonly neglected in transport calculations. This contribution arises from the combined effects of strong lattice anharmonicity, low phonon frequencies, and the resulting large thermal phonon populations at finite temperature. These ingredients are characteristic of halide perovskites and, more generally, of soft polar anharmonic materials, suggesting that nonlinear electron-phonon effects may be relevant well beyond $CsPbI_3$. Our results therefore motivate further theoretical developments capable of treating nonlinear electron-phonon interactions beyond the present approximations, including anharmonic phonon renormalization, higher-order one-electron-n-phonon processes,

and short-range coupling. The framework introduced here and in Refs. [37,59] provides a first step toward such a more complete description.

M.H., I.Z., W.W., S.K., and J.T. acknowledge the Research Foundation Flanders (FWO), Files No. 1224724N, No. V472923N, No. 1120825N, No. G060820N, No. G0A9F25N, and No. G0AIY25N, for their funding of this research. C.F. and J.T. acknowledge support from the joint Austrian Science Fund (FWF) - FWO project I 4506. S.P. is a Research Associate of the Fonds de la Recherche Scientifique - FNRS. This publication was supported by the Walloon Region in the strategic axe FRFS-WEL-T.

Data availability. The first-principles data and postprocessing code used to generate Figs. 2 and 3 are publicly available online [82,83].

[1] L. Ranalli, C. Verdi, M. Zacharias, J. Even, F. Giustino, and C. Franchini, Electron mobilities in $SrTiO_3$ and $KTaO_3$: Role of phonon anharmonicity, mass renormalization, and disorder, Phys. Rev. Mater. **8**, 104603 (2024).

[2] D. M. Jang, K. Park, D. H. Kim, J. Park, F. Shojaei, H. S. Kang, J.-P. Ahn, J. W. Lee, and J. K. Song, Reversible halide exchange reaction of organometal trihalide perovskite colloidal nanocrystals for full-range band gap tuning, Nano Lett. **15**, 5191 (2015).

[3] S. D. Stranks and H. J. Snaith, Metal-halide perovskites for photovoltaic and light-emitting devices, Nat. Nanotechnol. **10**, 391 (2015).

[4] T. M. Brenner, D. A. Egger, L. Kronik, G. Hodes, and D. Cahen, Hybrid organic—inorganic perovskites: Low-cost semiconductors with intriguing charge-transport properties, Nat. Rev. Mater. **1**, 15007 (2016).

[5] A. Kojima, K. Teshima, Y. Shirai, and T. Miyasaka, Organometal halide perovskites as visible-light sensitizers for photovoltaic cells, J. Am. Chem. Soc. **131**, 6050 (2009).

[6] M. A. Green, A. Ho-Baillie, and H. J. Snaith, The emergence of perovskite solar cells, Nat. Photon. **8**, 506 (2014).

[7] H. Min, D. Y. Lee, J. Kim, G. Kim, K. S. Lee, J. Kim, M. J. Paik, Y. K. Kim, K. S. Kim, M. G. Kim, T. J. Shin, and S. Il Seok, Perovskite solar cells with atomically coherent interlayers on SnO_2 electrodes, Nature (London) **598**, 444 (2021).

[8] Z.-K. Tan, R. S. Moghaddam, M. L. Lai, P. Docampo, R. Higler, F. Deschler, M. Price, A. Sadhanala, L. M. Pazos, D. Credgington, F. Hanusch, T. Bein, H. J. Snaith, and R. H. Friend, Bright light-emitting diodes based on organometal halide perovskite, Nat. Nanotechnol. **9**, 687 (2014).

[9] X.-K. Liu, W. Xu, S. Bai, Y. Jin, J. Wang, R. H. Friend, and F. Gao, Metal halide perovskites for light-emitting diodes, Nat. Mater. **20**, 10 (2021).

[10] S. Poncé, M. Schlipf, and F. Giustino, Origin of low carrier mobilities in halide perovskites, ACS Energy Lett. **4**, 456 (2019).

[11] S. Poncé, W. Li, S. Reichardt, and F. Giustino, First-principles calculations of charge carrier mobility and conductivity in bulk semiconductors and two-dimensional materials, Rep. Prog. Phys. **83**, 036501 (2020).

[12] F. Giustino, Electron-phonon interactions from first principles, Rev. Mod. Phys. **89**, 015003 (2017).

[13] O. Yaffe, Y. Guo, L. Z. Tan, D. A. Egger, T. Hull, C. C. Stoumpos, F. Zheng, T. F. Heinz, L. Kronik, M. G. Kanatzidis, J. S. Owen, A. M. Rappe, M. A. Pimenta, and L. E. Brus, Local polar fluctuations in lead halide perovskite crystals, Phys. Rev. Lett. **118**, 136001 (2017).

[14] A. Gold-Parker, P. M. Gehring, J. M. Skelton, I. C. Smith, D. Parshall, J. M. Frost, H. I. Karunadasa, A. Walsh, and M. F. Toney, Acoustic phonon lifetimes limit thermal transport in methylammonium lead iodide, Proc. Natl. Acad. Sci. USA **115**, 11905 (2018).

[15] M. J. Schilcher, P. J. Robinson, D. J. Abramovitch, L. Z. Tan, A. M. Rappe, D. R. Reichman, and D. A. Egger, The significance of polarons and dynamic disorder in halide perovskites, ACS Energy Lett. **6**, 2162 (2021).

[16] X. Zhu and D. A. Egger, Effect of overdamped phonons on the fundamental band gap of perovskites, Phys. Rev. Lett. **134**, 016403 (2025).

[17] J. Yin, O. Hellman, and S. Poncé, Impact of anharmonicity on the carrier mobility of the Pb-free $CsSnBr_3$ perovskite, arXiv:2505.20092.

[18] J.-M. Lihm and S. Poncé, Beyond-quasiparticle transport with vertex correction: Self-consistent ladder formalism for electron-phonon interactions, Phys. Rev. X **16**, 011008 (2026).

[19] H. T. Yi, X. Wu, X. Zhu, and V. Podzorov, Intrinsic charge transport across phase transitions in hybrid organo-inorganic perovskites, Adv. Mater. **28**, 6509 (2016).

[20] S. Dastidar, S. Li, S. Y. Smolin, J. B. Baxter, and A. T. Fafarman, Slow electron–hole recombination in lead iodide perovskites does not require a molecular dipole, ACS Energy Lett. **2**, 2239 (2017).

[21] S. Shrestha, G. J. Matt, A. Osvet, D. Niesner, R. Hock, and C. J. Brabec, Assessing temperature dependence of drift mobility in methylammonium lead iodide perovskite single crystals, J. Phys. Chem. C **122**, 5935 (2018).

[22] E. M. Hutter and T. J. Savenije, Thermally activated second-order recombination hints toward indirect recombination in fully inorganic $CsPbI_3$ perovskites, ACS Energy Lett. **3**, 2068 (2018).

[23] A. Biewald, N. Giesbrecht, T. Bein, P. Docampo, A. Hartschuh, and R. Ciesielski, Temperature-dependent ambipolar charge carrier mobility in large-crystal hybrid halide perovskite thin films, ACS Appl. Mater. Interfaces **11**, 20838 (2019).

[24] S. Sarkar, S. Banerjee, A. Swarnkar, and P. Mandal, Effect of capping ligand engineering on transport properties and carrier dynamics in cubic $CsPbI_3$ nanocrystal film, J. Phys. Chem. C **125**, 10539 (2021).

[25] C. Q. Xia, J. Peng, S. Poncé, J. B. Patel, A. D. Wright, T. W. Crothers, M. Uller Rothmann, J. Borchert, R. L. Milot, H. Kraus, Q. Lin, F. Giustino, L. M. Herz, and M. B. Johnston, Limits to electrical mobility in lead-halide perovskite semiconductors, J. Phys. Chem. Lett. **12**, 3607 (2021).

[26] H. Zhang, E. Debroye, J. A. Steele, M. B. J. Roeffaers, J. Hofkens, H. I. Wang, and M. Bonn, Highly mobile large polarons in black phase $CsPbI_3$, ACS Energy Lett. **6**, 568 (2021).

[27] Y. J. Lee, J. S. Han, D. E. Lee, T. H. Lee, J. Y. Kim, J. M. Suh, J. H. Lee, I. H. Im, S. J. Kim, K. J. Kwak, and H. W. Jang, High hole mobility inorganic halide perovskite field-effect transistors with enhanced phase stability and interfacial defect tolerance, Adv. Electron. Mater. **8**, 2100624 (2022).

[28] W. A. Saidi, S. Poncé, and B. Monserrat, Temperature dependence of the energy levels of methylammonium lead iodide perovskite from first-principles, J. Phys. Chem. Lett. **7**, 5247 (2016).

[29] M. Z. Mayers, L. Z. Tan, D. A. Egger, A. M. Rappe, and D. R. Reichman, How lattice and charge fluctuations control carrier dynamics in halide perovskites, Nano Lett. **18**, 8041 (2018).

[30] K. L. Ngai, Two-phonon deformation potential and superconductivity in degenerate semiconductors, Phys. Rev. Lett. **32**, 215 (1974).

[31] Yu. N. Epifanov, A. P. Levanyuk, and G. M. Levanyuk, Interaction of carriers with TO-phonons and electrical conductivity of ferroelectrics, Ferroelectrics **35**, 199 (1981).

[32] D. van der Marel, F. Barantani, and C. W. Rischau, Possible mechanism for superconductivity in doped $SrTiO_3$, Phys. Rev. Res. **1**, 013003 (2019).

[33] D. E. Kiselov and M. V. Feigel'man, Theory of superconductivity due to Ngai's mechanism in lightly doped $SrTiO_3$, Phys. Rev. B **104**, L220506 (2021).

[34] A. Kumar, V. I. Yudson, and D. L. Maslov, Quasiparticle and nonquasiparticle transport in doped quantum paraelectrics, Phys. Rev. Lett. **126**, 076601 (2021).

[35] Kh. G. Nazaryan and M. V. Feigel'man, Conductivity and thermoelectric coefficients of doped $SrTiO_3$ at high temperatures, Phys. Rev. B **104**, 115201 (2021).

[36] R. Bianco and I. Errea, Non-perturbative theory of the electron-phonon coupling and its first-principles implementation, arXiv:2303.02621.

[37] Z. Dai and F. Giustino, Nonlinear electron-phonon interactions from first principles, Phys. Rev. B (2026).

[38] T. Yildirim, O. Gülseren, J. W. Lynn, C. M. Brown, T. J. Udovic, Q. Huang, N. Rogado, K. A. Regan, M. A. Hayward, J. S. Slusky, T. He, M. K. Haas, P. Khalifah, K. Inumaru, and R. J. Cava, Giant anharmonicity and nonlinear electron-phonon coupling in MgB_2: A combined first-principles calculation and neutron scattering study, Phys. Rev. Lett. **87**, 037001 (2001).

[39] A. Y. Liu, I. I. Mazin, and J. Kortus, Beyond Eliashberg superconductivity in MgB_2: Anharmonicity, two-phonon scattering, and multiple gaps, Phys. Rev. Lett. **87**, 087005 (2001).

[40] P. S. Riseborough, The small polaron with nonlinear electron-phonon interactions, Ann. Phys. **153**, 1 (1984).

[41] C. P. J. Adolphs and M. Berciu, Going beyond the linear approximation in describing electron-phonon coupling: Relevance for the Holstein model, Europhys. Lett. **102**, 47003 (2013).

[42] C. P. J. Adolphs and M. Berciu, Single-polaron properties for double-well electron-phonon coupling, Phys. Rev. B **89**, 035122 (2014).

[43] S. Li and S. Johnston, The effects of non-linear electron-phonon interactions on superconductivity and charge-density-wave correlations, Europhys. Lett. **109**, 27007 (2015).

[44] S. Li, E. A. Nowadnick, and S. Johnston, Quasiparticle properties of the nonlinear Holstein model at finite doping and temperature, Phys. Rev. B **92**, 064301 (2015).

[45] D. M. Kennes, E. Y. Wilner, D. R. Reichman, and A. J. Millis, Transient superconductivity from electronic squeezing of optically pumped phonons, Nat. Phys. **13**, 479 (2017).

[46] M. A. Sentef, Light-enhanced electron-phonon coupling from nonlinear electron-phonon coupling, Phys. Rev. B **95**, 205111 (2017).

[47] P. M. Dee, J. Coulter, K. G. Kleiner, and S. Johnston, Relative importance of nonlinear electron-phonon coupling and vertex corrections in the Holstein model, Commun. Phys. **3**, 145 (2020).

[48] F. Grandi, J. Li, and M. Eckstein, Ultrafast Mott transition driven by nonlinear electron-phonon interaction, Phys. Rev. B **103**, L041110 (2021).

[49] J. Sous, B. Kloss, D. M. Kennes, D. R. Reichman, and A. J. Millis, Phonon-induced disorder in dynamics of optically pumped metals from nonlinear electron-phonon coupling, Nat. Commun. **12**, 5803 (2021).

[50] N. V. Prokof'ev and B. V. Svistunov, Phonon modulated hopping polarons: X-representation technique, Phys. Rev. B **106**, L041117 (2022).

[51] S. Ragni, T. Hahn, Z. Zhang, N. Prokof'ev, A. Kuklov, S. Klimin, M. Houtput, B. Svistunov, J. Tempere, N. Nagaosa, C. Franchini, and A. S. Mishchenko, Polaron with quadratic electron-phonon interaction, Phys. Rev. B **107**, L121109 (2023).

[52] Z. Zhang, A. Kuklov, N. Prokof'ev, and B. Svistunov, Soliton states from quadratic electron-phonon interaction, Phys. Rev. B **108**, 245127 (2023).

[53] Z. Han, S. A. Kivelson, and P. A. Volkov, Quantum bipolaron superconductivity from quadratic electron-phonon coupling, Phys. Rev. Lett. **132**, 226001 (2024).

[54] K. Kovač, D. Golež, M. Mierzejewski, and J. Bonča, Optical manipulation of bipolarons in a system with nonlinear electron-phonon coupling, Phys. Rev. Lett. **132**, 106001 (2024).

[55] S. N. Klimin, J. Tempere, M. Houtput, S. Ragni, T. Hahn, C. Franchini, and A. S. Mishchenko, Analytic method for quadratic polarons in nonparabolic bands, Phys. Rev. B **110**, 075107 (2024).

[56] S. Ragni, T. Miškić, T. Hahn, N. Prokof'ev, O. S. Barišić, N. Nagaosa, C. Franchini, and A. S. Mishchenko, Polarons with arbitrary nonlinear electron-phonon interaction, Phys. Rev. Res. **7**, 043304 (2025).

[57] M. A. Smondyrev, Diagrams in the polaron model, Theor. Math. Phys. **68**, 653 (1986).

[58] N.-E. Lee, J.-J. Zhou, H.-Y. Chen, and M. Bernardi, Ab initio electron-two-phonon scattering in GaAs from next-to-leading order perturbation theory, Nat. Commun. **11**, 1607 (2020).

[59] M. Houtput, L. Ranalli, C. Verdi, S. Klimin, S. Ragni, C. Franchini, and J. Tempere, First-principles theory of nonlinear long-range electron-phonon interaction, Phys. Rev. B **111**, 184320 (2025).

[60] Y. Yamada and Y. Kanemitsu, Electron-phonon interactions in halide perovskites, NPG Asia Mater. **14**, 48 (2022).

[61] See Supplemental Material at http://link.aps.org/supplemental/10.1103/jl6h-yzky for further derivations.

[62] G. Brunin, H. P. C. Miranda, M. Giantomassi, M. Royo, M. Stengel, M. J. Verstraete, X. Gonze, G.-M. Rignanese,

and G. Hautier, Electron-phonon beyond Fröhlich: Dynamical quadrupoles in polar and covalent solids, Phys. Rev. Lett. **125**, 136601 (2020).

[63] V. A. Jhalani, J.-J. Zhou, J. Park, C. E. Dreyer, and M. Bernardi, Piezoelectric electron-phonon interaction from *ab initio* dynamical quadrupoles: Impact on charge transport in wurtzite GaN, Phys. Rev. Lett. **125**, 136602 (2020).

[64] J. Lafuente-Bartolome, C. Lian, and F. Giustino, Topological polarons in halide perovskites, Proc. Natl. Acad. Sci. USA **121**, e2318151121 (2024).

[65] S. Poncé, E. R. Margine, and F. Giustino, Towards predictive many-body calculations of phonon-limited carrier mobilities in semiconductors, Phys. Rev. B **97**, 121201(R) (2018).

[66] H. Lee, S. Poncé, K. Bushick, S. Hajinazar, J. Lafuente-Bartolome, J. Leveillee, C. Lian, J.-M. Lihm, F. Macheda, H. Mori, H. Paudyal, W. H. Sio, S. Tiwari, M. Zacharias, X. Zhang, N. Bonini, E. Kioupakis, E. R. Margine, and F. Giustino, Electron–phonon physics from first principles using the EPW code, npj Comput. Mater. **9**, 156 (2023).

[67] H. Fröhlich, Electrons in lattice fields, Adv. Phys. **3**, 325 (1954).

[68] A. Miglio, V. Brousseau-Couture, E. Godbout, G. Antonius, Y.-H. Chan, S. G. Louie, M. Côté, M. Giantomassi, and X. Gonze, Predominance of non-adiabatic effects in zero-point renormalization of the electronic band gap, npj Comput. Mater. **6**, 167 (2020).

[69] B. Guster, P. Melo, B. A. A. Martin, V. Brousseau-Couture, J. C. de Abreu, A. Miglio, M. Giantomassi, M. Côté, J. M. Frost, M. J. Verstraete, and X. Gonze, Fröhlich polaron effective mass and localization length in cubic materials: Degenerate and anisotropic electronic bands, Phys. Rev. B **104**, 235123 (2021).

[70] G. Kresse and J. Furthmüller, Efficiency of ab-initio total energy calculations for metals and semiconductors using a plane-wave basis set, Comput. Mater. Sci. **6**, 15 (1996).

[71] G. Kresse and J. Furthmüller, Efficient iterative schemes for ab initio total-energy calculations using a plane-wave basis set, Phys. Rev. B **54**, 11169 (1996).

[72] D. Trots and S. Myagkota, High-temperature structural evolution of caesium and rubidium triiodoplumbates, J. Phys. Chem. Solids **69**, 2520 (2008).

[73] A. Togo, First-principles phonon calculations with phonopy and phono3py, J. Phys. Soc. Jpn. **92**, 012001 (2023).

[74] A. Togo, L. Chaput, T. Tadano, and I. Tanaka, Implementation strategies in phonopy and phono3py, J. Phys.: Condens. Matter **35**, 353001 (2023).

[75] I. Souza, J. Íñiguez, and D. Vanderbilt, First-principles approach to insulators in finite electric fields, Phys. Rev. Lett. **89**, 117602 (2002).

[76] Y. Su, K.-K. Song, M. Zhong, L.-B. Shi, and P. Qian, Stability and phonon-limited mobility for $CsSnI_3$ and $CsPbI_3$, J. Alloys Compd. **889**, 161723 (2021).

[77] H.-Y. Gu, W.-J. Yin, and X.-G. Gong, Significant phonon anharmonicity drives phase transitions in $CsPbI_3$, Appl. Phys. Lett. **119**, 191101 (2021).

[78] Y. Cao, G. Qi, C. Liu, L. Wang, Z. Ma, K. Wang, F. Du, G. Xiao, and B. Zou, Pressure-tailored band gap engineering and structure evolution of cubic cesium lead iodide perovskite nanocrystals, J. Phys. Chem. C **122**, 9332 (2018).

[79] G. D. Mahan, *Many Particle Physics*, 3rd ed., Physics of Solids and Liquids (Kluwer Academic/Plenum Pub, New York, 2000).

[80] M. Fu, P. Tamarat, J.-B. Trebbia, M. I. Bodnarchuk, M. V. Kovalenko, J. Even, and B. Lounis, Unraveling exciton–phonon coupling in individual $FAPbI_3$ nanocrystals emitting near-infrared single photons, Nat. Commun. **9**, 3318 (2018).

[81] J.-M. Lihm and S. Poncé, Nonperturbative self-consistent electron-phonon spectral functions and transport, Phys. Rev. Lett. **134**, 186401 (2025).

[82] https://github.com/MHoutput/1e2ph-spectral/.

[83] M. Houtput, I. Zappacosta, W. Wenborn, S. Klimin, S. Poncé, J. Tempere, and C. Franchini, Importance of nonlinear long-range electron-phonon interaction for the carrier mobility of anharmonic halide perovskites, Materials Cloud, 2026, https://doi.org/10.24435/materialscloud:5x-vd.